ISSN 1067-8212, Russian Journal of Non-Ferrous Metals, 2018, Vol. 59, No. 4, pp. 458–464. © Allerton Press, Inc., 2018.

REFRACTORY, CERAMIC, AND COMPOSITE MATERIALS

Synthesis, Corrosion and Bioactivity Evaluation of Gelatin/Silicon and Magnesium Co-Doped Fluorapatite Nanocomposite Coating Applied on AZ31 Mg Alloy[1]

Aliakbar Jafarzadeh[a, b], Tahmineh Ahmadi[a, b,*,], Majid Taghian Dehaghani[c], and Kamran Mohemi[a, b]**

[a] *Department of Materials Engineering, Shahreza Branch, Islamic Azad University, Shahreza, Isfahan, 86145-311, Iran*

[b] *Razi Chemistry Research Center (RCRC), Shahreza Branch, Islamic Azad University, Isfahan, Iran*

[c] *Department of Materials Engineering, Isfahan University of Technology, Isfahan, 8415683111 Iran*

**e-mail: tahmadi56@yahoo.com*

***e-mail: tahmineh.ahmadi@iaush.ac.ir*

Received October 25, 2017

Abstract—In this study, a nano-composite composed of gelatin as the matrix and Si-Mg-FA nano-particles as an additive was deposited on the AZ31 Mg alloy via dip coating method. In addition, a coating composed of MgO, $MgSiO_3$ and Mg_2SiO_4 phases was applied on the AZ31 Mg alloy by anodizing process. It was found that the Nano-composite coating with a uniform distribution of nano-particles within the gelatin matrix with the thickness of about 9 μm was dense, crack-free and uniform whereas the surface of anodized layer was relatively coarse due to the presence of flaws and micro-cracks. The surface morphology, EDS analysis and FTIR results revealed the ability of nano-composite coated specimen to form the bone-like apatite. Due to the presence of aforementioned phases and special surface features, the anodized specimen possessed higher and lower corrosion resistance than uncoated and nano-composite coated specimens, respectively. The passive coating resistances (R_{CT}) of nano-composite, anodized specimen and uncoated samples were 2164, 1449 and 1024 Ω cm^2, respectively.

Keywords: anodized, corrosion, bioactivity, dip coating, nano-composite

DOI: 10.3103/S1067821218040077

1. INTRODUCTION

Mg and its alloys exhibit some desirable properties that appoint them as implant materials for various medical applications. Mg, which is mainly present in the bones and is the fourth most abundant mineral element in human, is needed for human metabolism [1–3]. Magnesium and its alloys possess favorable mechanical properties such as a high ratio of strength to weight, a low density in comparison to many metals, and higher ductility compared to bio-ceramics [4, 5]. Furthermore, the elastic modulus of magnesium is lower than many metals such as stainless steels (189–205 GPa) and cobalt-chromium alloys (230 GPa), and is close to the natural bone [6]. This latter property leads to the reduction of stress shielding effect and avoidance of bone loss surrounding the implant [7]. Apart from these advantages, there are also some limitations to apply magnesium as an implant material. The first limitation is its weak corrosion resistance due to its highly negative equilibrium potential. The degradation rate is too rapid, which fails to complete the restoration of bone tissue [7]. The second problem with its application arises from the release of high amount of hydrogen gas during corrosion, leading to a balloon effect [8]. The third and final limitation is related to the low bioactivity of these alloys [9].

To improve the corrosion behavior and to increase the bioactivity of magnesium alloys, surface treatment through deposited coatings and conversion coatings are possible methods. Anodization coating is a kind of conversion coating, which is constituted by interaction of metal with aqueous solutions. In this technique, the in situ protective layers on magnesium with a porous structure are grown during dissolution and precipitation of ions in an aqueous electrolyte solution by connecting the component to a high-voltage power source typically up to 100 V [10, 11]. The anodized layer is mostly a blend of ceramics phases such as silicates and oxides. For organic thin layer, dip coating technique, which is a type of deposited coating, has been introduced as a common method. In this method, the substrate is vertically dipped in a solution bath (coating

[1] The article is published in the original.

bath) and then it is slightly withdrawn at a constant rate. The layer thickness is determined by the viscosity of the slurry, withdrawal speed, temperature and atmospheric conditions. Low temperature, quick and simple processing, inexpensive, uniform thin layer, large sizes and complicated shapes of substrate are among the advantages in selecting this technique [12, 13].

Among the natural biopolymers, gelatin, which is typically obtained from bovine, porcine skin or hydrolysis of collagen, is a very attractive and common one utilized in a wide range of clinical applications [14]. On the other hand, in our previous investigation, F (Fluorine), Mg (Magnesium) and Si (Silicon) were incorporated into the HA (hydroxyl apatite) structure to stimulate the formation of biological apatite. The results show that by substituting the Si and Mg, the solubility of Si–Mg–FA nano-powders was increased in comparison to FA (Fluorapatite); therefore, the adsorption of Ca^{2+} ions onto the powders' surfaces was simultaneously increased [15].

In this work, efforts have been made to adjust corrosion rate and provide precipitation ability of apatite layer by using Gelatin/Mg-Si-FA nano-composite on AZ31 Mg alloy. In addition, the corrosion behavior of uncoated, anodized, and nano-composite coated specimens were compared with each other.

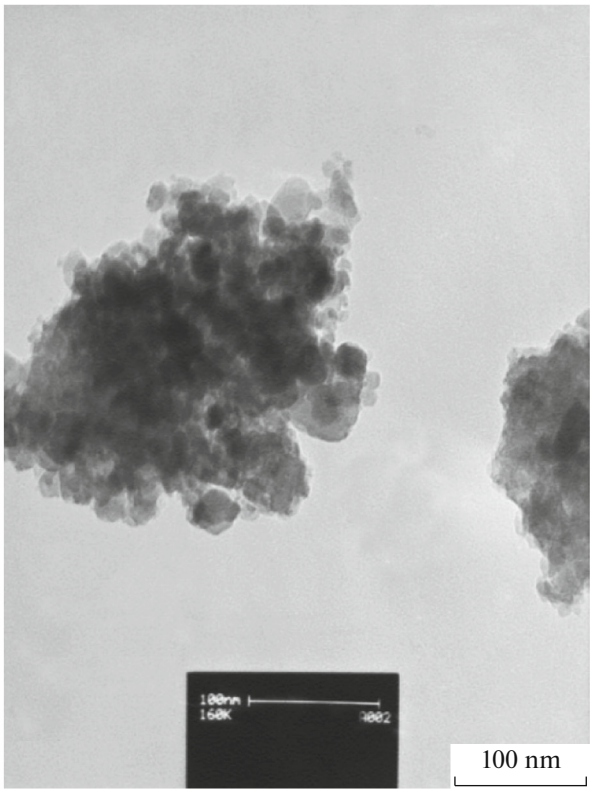

Fig. 1. TEM image of Si–Mg–FA nano-particles.

2. EXPERIMENTAL

2.1. Dip Coating Process

AZ31 Mg alloy ingots with composition of 0.02% Si, 0.44% Mn, 0.92% Zn, 2.7% Al, and 91.84% Mg were cut to a size of 5 × 10 × 10 mm. The specimens were ground with abrasive papers up to 400 mesh and then they were ultrasonically washed with distilled water for 20 min, alcohol for 20 min and acetone for 20 min in turn.

Silicon and magnesium co-doped fluorapatite (Si–Mg–FA) nano-powder was synthesized according to the experimental procedure described in our previous study [15]. The transmission electron microscopy (TEM; CM120, Philips) image of synthesized Si–Mg–FA nano-particles shown in Fig. 1 indicates that the nano-particles have spherical shapes with a mean diameter of about 30 nm.

To prepare the Gelatin/Mg–Si–FA nano-composite, first, 0.05 g of synthesized Mg–Si–FA nano-powder and 0.5 g of gelatin (Sigma, type A) were mixed with 10 mL of double distilled water. The nano-particles were well dispersed in solution in an ultrasonic bath for 2 h. Then, 0.16 g of EDC solution containing 9 cc ethanol and 1 cc double distilled water was added to the nano-powder suspension and the resulting solution was magnetically stirred for 8 h. The nano-composite coatings were deposited on the prepared AZ31 Mg alloy specimens by dip coating technique. In this way, the specimens were dipped in and pulled out of the nano-composite solution with a rate of 1 mm/s three times by using a completely automated control system.

2.2. Anodizing Process

316L stainless steel plates (10 × 20 × 1 mm) and aforementioned AZ31 Mg alloy specimens were polished with abrasive papers up to 1200 mesh and were used as cathode and anode electrodes, respectively. The anodizing process was carried out in an electrolytic solution containing 100 g/L NaOH, 100 g/L Na_2SiO_3 and 20 g/L KOH (aqueous solution), applying voltage and time of 30 V and 30 min, respectively. The distance between anode and cathode was fixed at 2 cm. The anodized samples were ultrasonically cleaned by distilled water and acetone and were dried in air.

2.3. Characterization

For bioactivity evaluation of nano-composite coated specimens, simulated body fluid (SBF) was used. This solution, prepared according to Kokubo's procedure, has ions concentration nearly equal to that of the human blood plasma [16]. Specimens soaked in this solution were maintained under physiological condition of pH 7.41 at 37 ± 0.5°C for 28 days. Surface

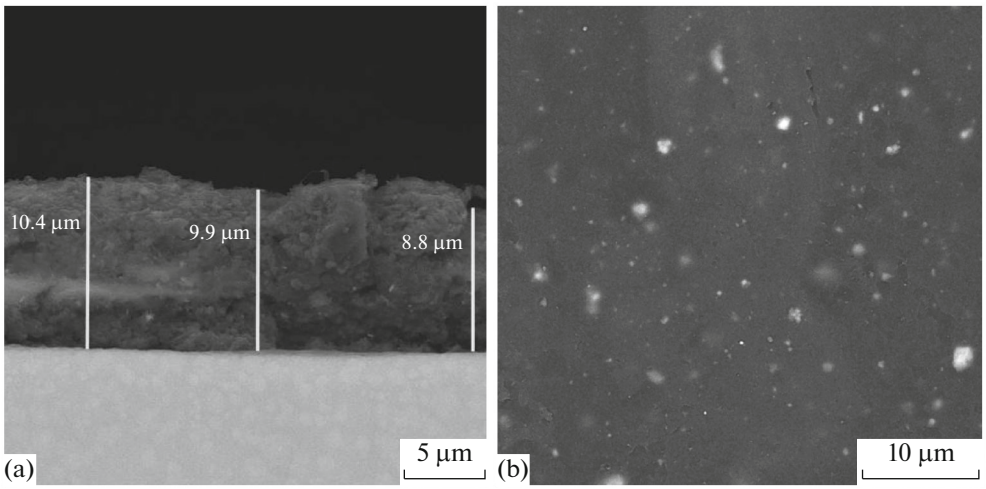

Fig. 2. SEM images of (a) cross section and (b) surface of Gelatin/Si–Mg–FA coating.

area (mm^2) of specimen ratio to SBF solution volume (mL) was set to be 1:10 [16].

The electrochemical tests of uncoated, anodized and nano-composite coated specimens were performed by potentiodynamic polarization and electrochemical impedance spectroscopy (EIS) in SBF solution using a conventional three-electrode cell at room temperature. A saturated Ag/AgCl electrode, 1 cm^2 of specimen and platinum electrode were used as reference, working and counter electrodes, respectively. The electrodes were connected to a corrosion measurement instrument (Ivium). Before starting the tests, the specimens were held at open circuit potential (OCP) for 1 h. The potentiodynamic polarization scans started at 250 mV below the corrosion potential at a scan rate of 1 mV/s. For electrochemical impedance spectroscopy measurements, a sinusoidal potential signal of 3.53 mV (rms) was applied as the amplitude of the perturbation signal, with a frequency range between 100 kHz and 10 mHz.

Surface morphology of Gelatin/Si–Mg–FA coating before and after immersion in SBF solution, anodized AZ31 Mg alloy, cross sectional morphology of Gelatin/Si–Mg–FA coating and Si–Mg–FA nanoparticles distribution within the composites matrices coating were evaluated by scanning electron microscopy (SEM; Mira 3-XMU) equipped with an energy-dispersive X-ray spectroscopy (EDXS).

The AZ31 Mg substrate, anodized and Gelatin/Si–Mg–FA coated specimens were analyzed for their phase present by a Philips X'Pert X-ray diffractometer (XRD) operating with CuK_α radiation (λ = 0.1542 nm) at 45 kV with a step size of 0.02° and time per step of 1 s in the range of 30°–80°.

Fourier transform infrared spectroscopy (FTIR) was used to examine the chemical structure of the specimens before and after immersion in SBF solution. FTIR Spectrum (65-Perkin Elmer) analysis was performed at resolution of 1 cm^{-1} using KBr pellet technique in the range of 450–4000 cm^{-1}.

3. RESULTS AND DISCUSSION

Figures 2a, 2b shows the cross-section and top view of Gelatin/Si–Mg–FA coating. From these figures, it can be observed that a dense, crack-free, well-compacted and uniform Gelatin/Si–Mg–FA layer with the thickness of about 9 μm has been performed on AZ31 Mg substrate. The absence of gap in the interface of substrate and coating and/or the absence of delamination could indicate that nano-composite coating has adhered well on the substrate. Moreover, a homogeneous distribution of nano-particles throughout the Gelatin matrix has been achieved.

Figures 3a, 3b shows surface morphology and X-ray diffraction pattern of anodized AZ31 Mg alloy, respectively. From Fig. 3a, it can be seen that the anodized layer has a large number of flaws, micro-cracks and micro-pores. Because of the presence of these features, the surface of anodized film is relatively coarse, which is the characteristic feature of anodized films. During the anodizing process, discharging sparks on the local region of the surface lead to break down the surface dielectric layer and melt the discharge channels. Local stresses due to preferential growth of anodized layer, composition and phase changes and fast solidification of molten oxides in contact with the electrolyte solution cause the formation of aforementioned special surface features [7, 17]. In addition, the birth and trapping of gas bubbles such as oxygen and hydrogen because of chemical reactions are other reasons for the formation of micro-pores and defects [18]. XRD pattern shown in Fig. 3b confirms the chemical reactions, composition and phase changes after anodizing process. This pattern shows that the anodic film is composed of MgO, $MgSiO_3$,

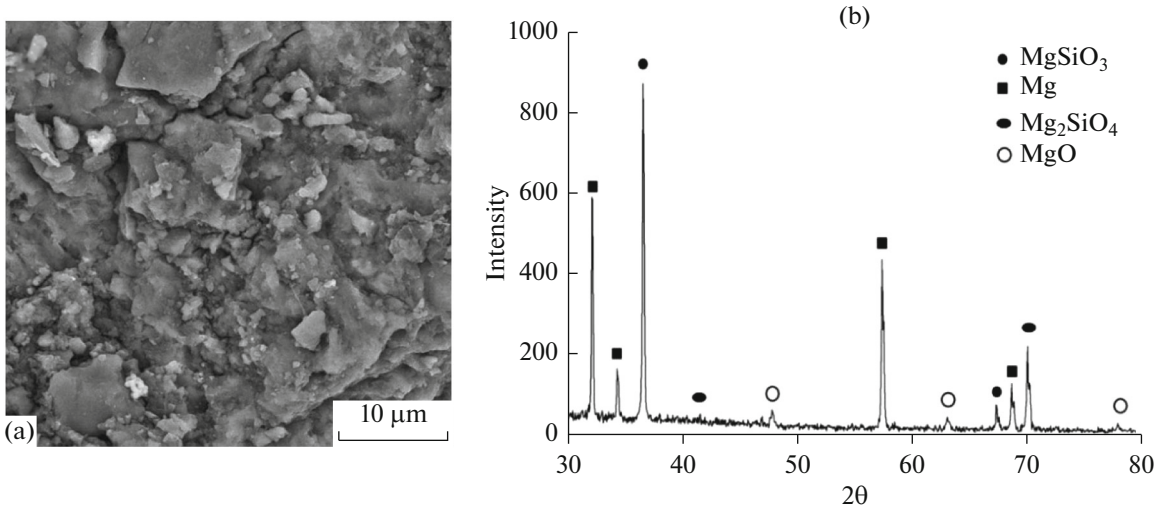

Fig. 3. (a) SEM image and (b) X-ray diffraction pattern of anodized AZ31 Mg alloy.

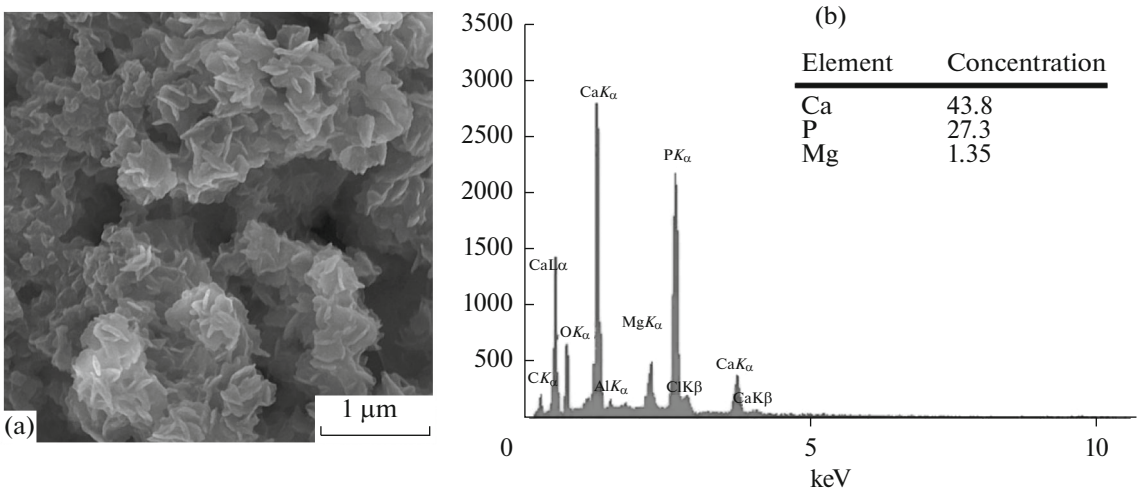

Fig. 4. (a) SEM image of Gelatin/Si–Mg–FA coated AZ31 Mg alloy substrate after soaking in SBF for 28 days showing apatite crystals and (b) EDS spectrum of these particles.

Mg_2SiO_4, and Mg phases. MgO phase is a result of the direct reaction between Magnesium and active oxygen in electrolyte. During the anodizing process, the reactions between $Si(OH)_4$ groups, which come from the hydroxylation of SiO^{-3} in aqueous solution, lead to the formation of SiO_2 phase. Considering the high temperature at sparking areas on the Mg substrate surface, $MgSiO_3$ and Mg_2SiO_4 are formed by the reaction between SiO_3^{-2} and Mg^{+2} and between SiO_2 and MgO, respectively.

The main aim of applying Gelatin/Si–Mg–FA nano-composite coating on the surface of AZ31 Mg alloy is to improve its corrosion and bioactivity properties. The immersion test in SBF solution was performed to evaluate the ability of the specimen to form the bone-like apatite. SEM image of nano-composite coated sample immersed in SBF solution for 28 days is shown in Fig. 4a. This image reveals that during soaking, a surface reaction occurs between the coating and solution. The surface is completely covered by a reaction layer. As can be seen, the morphology of this reaction layer, arisen from the dissolution–precipitation process, is cloud-like morphology, which is the typical morphology of apatite phase. The result of EDS spectrum shown in Fig. 4b exhibits that this reaction layer mostly includes Mg, Ca, P and O, which implies formation of apatite crystals [19]. To obtain further confidence of apatite phase existing on the surface of coated specimen after immersion in SBF solution, FTIR analysis was also conducted. FTIR spectra of nano-composite coated samples before and after

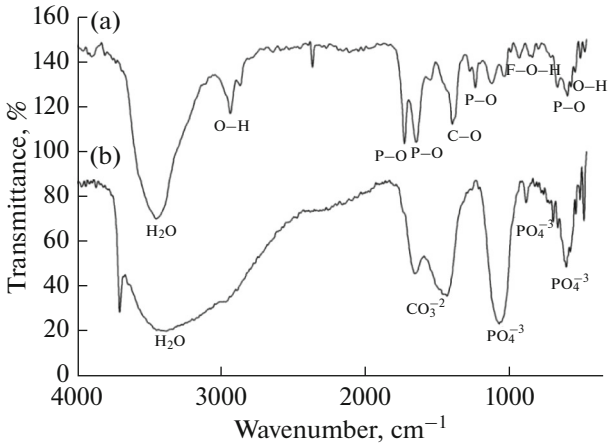

Fig. 5. FTIR spectra of Gelatin/Si–Mg–FA nano-composite coating (a) before and (b) after soaking in SBF for 28 days.

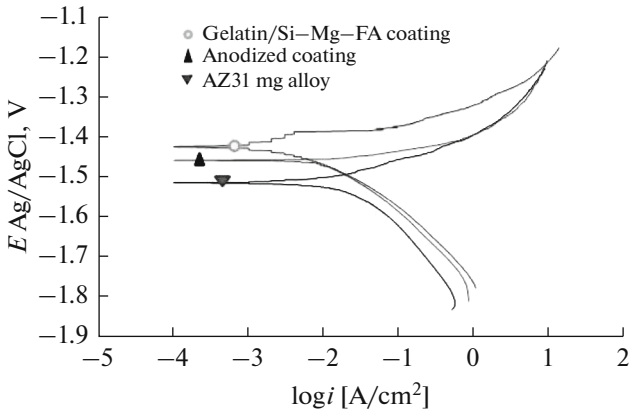

Fig. 6. The potentiodynamic polarization curves of uncoated, anodized, Gelatin/Si–Mg–FA coated samples in SBF solution.

immersion in SBF are shown in Fig. 5. Characteristic structural bands of gelatin and Si-Mg-FA nano-particles were present in the FTIR spectrum of specimen before immersion in SBF. As can be seen, two characteristic absorption peaks at about 1565 and 1650 cm^{-1} correspond to amide I band and II band of gelatin. Peptide linkages in the protein, which is the stretching vibrations of C–O bond leading to amide I band and amide II band, are caused by coupling the stretching of the C–N bonds and the N–H bond in plane bending. Furthermore, the absorption peak located at 2937 cm^{-1} is derived from the stretching of methyl group of C–H bond of gelatin. P–O bands at 512 and 1055 cm^{-1} assigned to the bending and the asymmetrical stretching modes, and Carbonate peak at 840 cm^{-1} for the bending modes are attributed to Si–Mg–FA nano-particles. The presence of O–H peaks is attributed to the water adsorbed in apatite lattice in the sample and/or in the KBr pellet [20]. FTIR spectrum of Gelatin/Si–Mg–FA nano-composite coating after soaking in SBF for 28 days is shown in Fig. 5b. As can be seen, there are obviously significant differences in the functional groups between the FTIR spectra of specimens before and after immersion in the SBF solution. This spectrum confirms that these precipitates in the form of cloud-like particles with their characteristic phosphate and carbonate peaks are related to bone-like apatite. Phosphate peaks observed at 1050 and 605 cm^{-1} signify the phosphate absorption in crystalline state; and characteristic peaks at 1490 and 1426 cm^{-1} are also present corresponding to the carbonate bands.

The corrosion protection properties of uncoated, anodized and Gelatin/Si–Mg–FA nano-composite coated specimens were assessed through potentiodynamic polarization analysis (PDP) and electrochemical impedance spectroscopy (EIS) in SBF solution; and the recorded curves were evaluated. Polarization curves of specimens with and without coatings are observed in Fig. 6. The electrochemical corrosion parameters of the uncoated and coated specimens, including the corrosion current density (i_{corr}), the corrosion potential (E_{corr}) and anodic/cathodic Tafel slopes (βa and βc) derived from the polarization curves by extrapolating the anodic and cathodic branches are summarized and listed in Table 1.

In general, more E_{corr} values and less i_{corr} values indicate enhancement in corrosion resistivity [21]. As can be seen, the formation of anodized and nano-composite coating on the specimen result in shifting E_{corr} to the more positive values. Simultaneously, corrosion current densities of the coated specimens are shifted to a smaller amount in comparison to the uncoated specimen. The data in Table 1 reveals lower value of i_{corr} and higher values of E_{corr} in the case of the anodized specimen compared to the uncoated speci-

Table 1. The electrochemical corrosion parameters of uncoated, anodized, Gelatin/Si–Mg–FA coated samples derived from the polarization curves in in SBF solution

Specimen	β_a, V dec^{-1}	β_c, V dec^{-1}	E_{corr}, V	i_{corr}, A cm^{-2}
AZ31 Mg alloy	0.27	0.22	–1.68	2.98E-4
Anodized coat	0.17	0.18	–1.59	1.071E-4
Gelatin/Si–Mg–FA coat	0.07	0.14	–1.47	5.022E-5

Table 2. Electrochemical parameters of the uncoated and coated specimens obtained by equivalent circuit simulation

Specimen	R_s, Ω cm^2	R_{CT}, Ω cm^2	n	i_0, A cm^{-2}
AZ31 Mg alloy	23.8	1024	0.87	2.3×10^{-3}
Anodized coat	23.3	1449	0.86	2.5×10^{-5}
Gelatin/Si–Mg–FA coat	25.3	2164	0.83	1.8×10^{-5}

men. As indicated by XRD pattern shown in Fig. 3b, the anodized layer is mainly composed of MgO, $MgSiO_3$ and $Mg_2(SiO_4)$ phases. This implies that these ceramic phases can act as a barrier layer to reduce electron and ions diffusion, therefore, leading to a reduction in the electrochemical reactions at the interface of Mg alloy and electrolyte. On the other hand, it is obvious that compared to the anodized specimen, the i_{corr} value of nano-composite coated specimen is considerably lower. This value shows more effective role of nano-composite coating in reducing the electron transfer and better corrosion resistance in comparison to anodized coating. The Nyquist plot for the uncoated, anodized and Gelatin/Si–Mg–FA coated specimens in the SBF solution are shown in Fig. 7a. The equivalent circuit drawn in Fig. 7b was applied to simulate the EIS results. This equivalent circuit consists of a solution resistance (R_S), the passive coating resistance (R_{CT}) and constant-phase element (CPE). The values of these simulated parameters computed by curve-fit using the equivalent circuit are summarized in Table 2. R_{CT}, the most important parameter, is proportional to the diameter of capacitive semicircle at the high frequency region. In addition, based on the following equation, R_{CT} is inversely proportional to the exchange-current density (i_0) [22]:

$$R_{CT} = RT/nFi_0. \quad (4)$$

Where F is Faraday constant and n is the number of transferred charges. Thus, the higher R_{CT} means the lower i_0 and better corrosion resistivity. As can be seen, the Nyquist curves of the uncoated and coated specimens exhibit a single semicircle at all high frequencies, and the loop of the nano-composite coating has a larger diameter in comparison to uncoated and anodized specimens. According to Table 2, the R_{CT} values for three specimens in ascending order are uncoatd < anodized < nano-composite coating. The nano-composite coated specimen exhibits higher R_{CT} value than the uncoated and anodized specimens, suggesting that the corrosion resistance of the nano-composite coated specimen is enhanced. It is worth mentioning that the impedance of all the specimens decreases with increasing frequency so that they have the same impedance at high frequency, revealing either diffusion or capacitive attributes. However, the EIS results in agreement with polarization measurement outcomes show high corrosion protection of nano-composite coating against corrosive ions diffusion. This excellent corrosion resistivity of nano-composite coating could be due to the effect of gelatin as an electrical insulator, sealing the substrate from the corrosion electrolyte ions. Another reason for the improvement of the corrosion resistance is due to the uniform, crack-free and dense structure of this coating as confirmed by SEM shown in Fig. 2b. The incorporation of Si–Mg–FA nano-particles as inert physical barriers into the gelatin can result in the denser coating by filling the submicron defects [23].

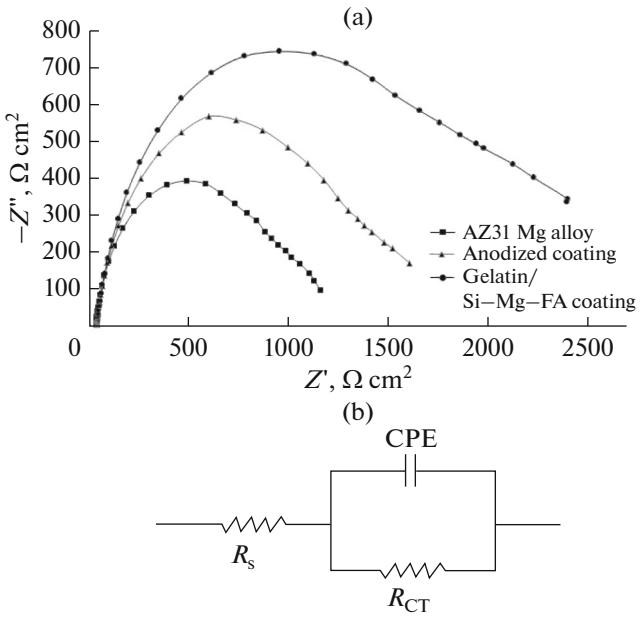

Fig. 7. (a) Nyquist plot for uncoated, anodized and Gelatin/Si–Mg–FA coated samples and (b) Electrical equiva lent circuit for the interpretation of the experimental EIS data.

4. CONCLUSIONS

Gelatin/Si–Mg–FA nano-composite coating was deposited on the AZ31 Mg alloy specimens by dip coating technique. The anodized coating was also formed on the AZ31 Mg alloy in an electrolytic aqueous solution containing NaOH, Na_2SiO_3 and KOH.

Nano-composite coating having a homogeneous distribution of nano-particles throughout the gelatin matrix was dense, crack-free, well compacted and uniform whereas because of the presence of flaws, microcracks and micro-pores the surface of anodized layer was relatively coarse. The immersion test of nanocomposite coated specimens in SBF solution reveals the ability of these specimens to form the bone-like apatite. The results of the electrochemical tests showed more effective role of nano-composite coating in the improvement of corrosion resistance in comparison to uncoated and anodized specimens. In summary, the present investigation has shown that Gelatin/Si–Mg–FA nano-composite coating could be a good candidate to use as a bioactive and corrosion resistant nano-composite in order to control the corrosion rate of Mg alloys for bone engineering.

REFERENCES

1. Yang, L. and Zhang, E., Biocorrosion behavior of magnesium alloy in different simulated fluids for biomedical application, *Mater. Sci. Eng. C*, 2009, vol. 29, pp. 1691–1696.
2. Staiger, M.P., Pietak, A.M., Huadmai, J., et al., Magnesium and its alloys as orthopedic biomaterials: a review, *Biomaterials*, 2006, vol. 27, pp.1728–1734.
3. Zhao, L., Cui, C., Wang, Q., et al., Growth characteristics and corrosion resistance of micro-arc oxidation coating on pure magnesium for biomedical applications, *Corros. Sci.,* 2010, vol. 52, pp. 2228–2234.
4. Degnera, J., Singer, F., Cordero, L., et al., Electrochemical investigations of magnesium in DMEM with biodegradable polycaprolactone coating as corrosion barrier, *Appl. Surf. Sci.*, 2013, vol. 282, pp. 264–270.
5. Chai, L., Yu, X., Yang, Z., et al., Anodizing of magnesium alloy AZ31 in alkaline solutions with silicate under continuous sparking, *Corros. Sci.*, 2008, vol. 50, pp. 3274–3279.
6. Razavi, M., Fathi, M., Savabi, O., et al., A review of degradation properties of Mg based biodegradable implants, *Res. Rev. Mater. Sci. Chem.*, 2012, vol. 1, pp. 15–58.
7. Wang, Y.M., Guo, J.W., Shao, Z.K., et al., A metasilicate-based ceramic coating formed on magnesium alloy by microarc oxidation and its corrosion in simulated body fluid, *Surf. Coat. Tech.*, 2013, vol. 219, pp. 8–14.
8. Wong, H.M., Yeung, K.W.K., Lam, K.O., et al., A biodegradable polymer-based coating to control the performance of magnesium alloy orthopedic implants, *Biomaterials*, 2010, vol. 31, pp. 2084–2096.
9. Razavi, M., Fathi, M., Savabi, O., et al., Micro-arc oxidation and electrophoretic deposition of nano-grain merwinite ($Ca_3MgSi_2O_8$) surface coating on magnesium alloy as biodegradable metallic implant, *Surf. Interface Anal.*, 2014, vol. 46, pp. 387–392.
10. Razavia, M., Fathi, M., Savabi, O., et al., Nanostructured merwinite bioceramic coating on Mg alloy deposited by electrophoretic deposition, *Ceram. Int.*, 2014, vol. 40, pp. 9473–9484.
11. Walsh, F.C., Low, C.T.J., Wood, R.J.K., et al., Plasma electrolytic oxidation (PEO) for production of anodised coatings on lightweight metal (Al, Mg, Ti) alloys, *Trans. IMF*, 2009, vol. 87, pp. 122–135.
12. Dadash, M.S., Karbasi, S., Esfahani, M.N., et al., Influence of calcinated and noncalcinated nanobioglass particles on hardness and bioactivity of sol–gel-derived TiO_2–SiO_2 nanocomposite coatings on stainless steel substrates, *J. Mater. Sci.–Mater. Med.*, 2011, vol. 22, pp. 829–838.
13. Dorozhkin, S.V., Bioceramics of calcium orthophosphates, *Biomaterials*, 2013, vol. 1, pp. 1465–1485.
14. Sell, S.A., Wolfe, P.S., Garg, K., et al., The Use of Natural Polymers in Tissue Engineering: A Focus on Electrospun Extracellular Matrix Analogues, *Polymers*, 2010, vol. 2, pp. 522–553.
15. Ahmadi, T., Monshi, A., Mortazavi, V., et al., Synthesis and dissolution behavior of nanosized silicon and magnesium co-doped fluorapatite obtained by high energy ball milling, *Ceram. Int.*, 2014, vol. 4, pp. 8341–8349.
16. Kokubo, T. and Takadama, H., How useful is SBF in predicting in vivo bone bioactivity?, *Biomaterials*, 2006, vol. 27, pp. 2907–2915.
17. Lia, L.H., Konga, Y.M., Kima, H.W., et al., Improved biological performance of Ti implants due to surface modification by micro-arc oxidation, *Biomaterials*, 2004, vol. 25, pp. 2867–2875.
18. Zhang, Y., Yan, C., Wang, F., and Li, W., Electrochemical behavior of anodized Mg alloy AZ91D in chloride containing aqueous solution, *Corros. Sci.*, 2005, vol. 47, pp. 2816–2831.
19. Xu, L., Zhang, E., Yin, D., et al., In vitro corrosion behavior of Mg alloys in a phosphate buffered solution for bone implant application, *J. Mater. Sci.–Mater. Med.*, 2008, vol. 19, pp. 1017–1025.
20. Hanifi, A., Fathi, M., Mir Mohammad Sadeghi, H., et al., Mg^{2+} substituted calcium phosphate nano particles synthesis for non-viral gene delivery application, *J. Mater. Sci.–Mater. Med.*, 2010, vol. 21, pp. 2393–2401.
21. Cui, X., Li, Y., Li, Q., et al., Influence of phytic acid concentration on performance of phytic acid conversion coatings on the AZ91D magnesium alloy, *Mater. Chem. Phys.*, 2008, vol. 111, pp. 503–507.
22. Udhayan, R. and Devendra, P.B., On the corrosion behaviour of magnesium and its alloys using electrochemical techniques, *J. Power Sources*, 1996, vol. 563, pp. 103–107.
23. Ashassi-Sorkhabi, H. and Eshaghi, M., Corrosion resistance enhancement of electroless Ni–P coating by incorporation of ultrasonically dispersed diamond nanoparticles, *Corros. Sci.*, 2013, pp. 77, pp. 185–193.